Measurement-Induced State Transitions in a Superconducting Qubit: Beyond the Rotating Wave Approximation

Daniel Sank,[1,*] Zijun Chen,[2] Mostafa Khezri,[3,4] J. Kelly,[1] R. Barends,[1] B. Campbell,[2] Y. Chen,[1] B. Chiaro,[2] A. Dunsworth,[2] A. Fowler,[1] E. Jeffrey,[1] E. Lucero,[1] A. Megrant,[1] J. Mutus,[1] M. Neeley,[1] C. Neill,[2] P. J. J. O'Malley,[2] C. Quintana,[2] P. Roushan,[1] A. Vainsencher,[1] T. White,[1] J. Wenner,[2] Alexander N. Korotkov,[3] and John M. Martinis[1,2]

[1]Google Inc., Santa Barbara, California 93117, USA

[2]Department of Physics, University of California, Santa Barbara, California 93106-9530, USA

[3]Department of Electrical and Computer Engineering, University of California, Riverside, California 92521, USA

[4]Department of Physics, University of California, Riverside, California 92521, USA

(Received 21 June 2016; published 4 November 2016)

Many superconducting qubit systems use the dispersive interaction between the qubit and a coupled harmonic resonator to perform quantum state measurement. Previous works have found that such measurements can induce state transitions in the qubit if the number of photons in the resonator is too high. We investigate these transitions and find that they can push the qubit out of the two-level subspace, and that they show resonant behavior as a function of photon number. We develop a theory for these observations based on level crossings within the Jaynes-Cummings ladder, with transitions mediated by terms in the Hamiltonian that are typically ignored by the rotating wave approximation. We find that the most important of these terms comes from an unexpected broken symmetry in the qubit potential. We confirm the theory by measuring the photon occupation of the resonator when transitions occur while varying the detuning between the qubit and resonator.

DOI: 10.1103/PhysRevLett.117.190503

The Jaynes-Cummings (JC) Hamiltonian [1,2] describes the interaction between a quantum two-level system (TLS) and a harmonic oscillator, and is used to model a huge variety of physical systems. For example, in superconducting qubits, it describes the interaction between the qubit and a resonator used to measure the qubit's state. As predicted by the dispersive limit of the JC model, each qubit state induces a different frequency shift in the resonator, and the qubit state is inferred by measuring the resonator's response to a probe pulse [3–5]. Dispersive measurement itself played a key role in recent experiments exploring the nature of quantum measurement [6–8], and the high speed and accuracy of dispersive measurement has been critical in establishing superconducting qubits as a compelling technology for quantum computation [9,10]. Furthermore, repetitive error protection and characterization protocols [11–16] require that the qubit remain in a known state within the qubit subspace after the measurement is complete, a property guaranteed by the dispersive JC Hamiltonian.

However, several experiments with superconducting qubits have found that as the number of photons occupying the resonator $\overline{n}$ is increased past a certain point, the qubit suffers anomalous state transitions [17–20]. It was long believed that these transitions could be explained by the breakdown of the dispersive approximation of the JC model as $\overline{n}$ exceeds a critical photon number n_c, but recent theory showed that the transitions are not predicted by the JC interaction even with very large $\overline{n}$ [21]. Perhaps more puzzling, the transition probability is observed to be nonmonotonic with increasing photon number. As these transitions limit the speed and lower the fidelity of qubit measurement [18,20], understanding and eliminating them is an important step in implementing high fidelity quantum algorithms, simulation, and error corrected computation.

In this Letter, we investigate the cause of anomalous qubit transitions in a superconducting qubit-resonator system. We characterize the transitions by measuring the state of the qubit after driving the resonator with variable power, and find that the qubit jumps outside the two-level subspace. Moreover, these transitions show a resonant behavior as a function of drive power. By reexamining an important assumption of the JC Hamiltonian, the rotating wave approximation (RWA), we develop a theory based on level crossings with other states of the qubit-resonator system, and find that the theory matches experimental observations with no free parameters.

Our experiment used a superconducting transmon qubit [5,22] capacitively coupled to the fundamental mode of a quarter wave coplanar waveguide resonator with coupling strength $g/2\pi \approx 87$ MHz [23], as illustrated in Fig. 1(a). The transmon's weakly anharmonic potential supports a ladder of energy levels, the bottom two of which are used as a qubit. By biasing the transmon's dc superconducting quantum interference device (SQUID) with a magnetic flux, we can tune the transmon's $|0\rangle \rightarrow |1\rangle$ transition frequency ω_{10}. In the absence of bias flux, the transmon has its maximum frequency $\omega_{10}/2\pi = 5.4$ GHz, and the anharmonicity is $\eta/2\pi \equiv (\omega_{21} - \omega_{10})/2\pi = -221$ MHz. The fundamental

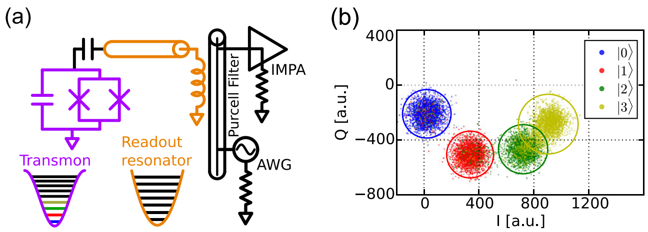

FIG. 1. Transmon-resonator system. (a) Circuit and potential diagrams. The transmon (violet) is capacitively coupled to the resonator (orange). The resonator is inductively coupled to a bandpass Purcell filter with $Q \approx 30$ [20]. The resonator is driven by an arbitrary waveform generator connected to the filter, and the dispersed photons are measured by a low noise, impedance matched parametric amplifier [25] also connected to the filter. (b) In-phase and quadrature (IQ) components of the dispersed signal measured with the transmon prepared in the first four states, with each state forming an IQ "cloud." The circles represent 3σ from fitting a Gaussian distribution to each cloud's projection onto lines connecting the clouds' centers.

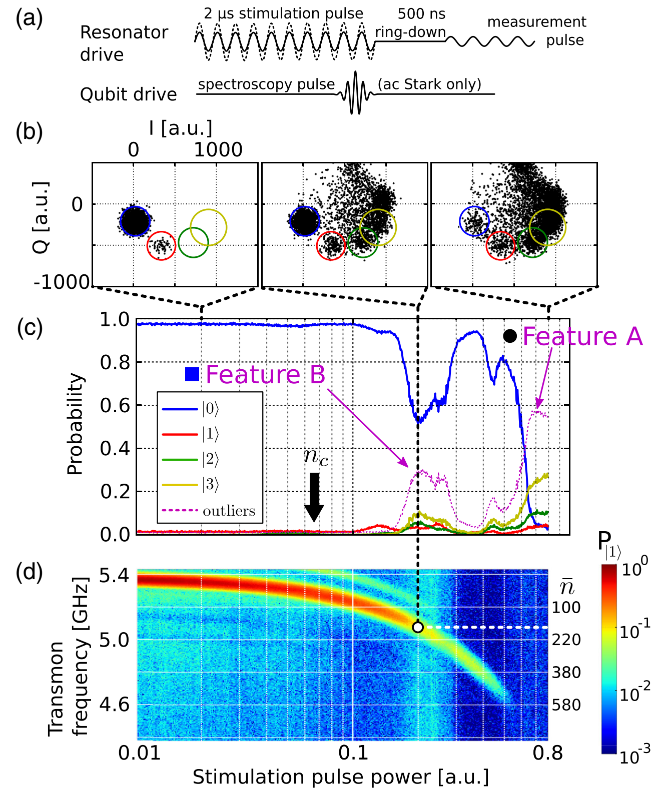

FIG. 2. (a) Control sequence for probing the effect of resonator photons on the transmon. The spectroscopy pulse is used only in the ac Stark measurement. (b) IQ data for drive powers 0.02, 0.2, and 0.8 (arbitrary units), with $\omega_{10} = 5.38$ GHz. The circles represent 3σ for the four resolvable transmon states as calibrated in Fig. 1(b). At high power, the transmon is clearly driven to states higher than $|3\rangle$. (c) Transmon state probabilities versus stimulation power. In addition to the four calibrated transmon states, we show the probability that the measurement was $> 3\sigma$ from any of the resolved states, labeled "outliers." Note the two large resonance shaped peaks labeled A and B. (d) Stark shifted transmon frequency ω_{10} versus stimulation pulse power. We convert the shifted ω_{10} to $\bar{n}$ using a numerical theory (right vertical axis) [28].

mode of the resonator is a quantum harmonic oscillator with frequency $\omega_r/2\pi \approx 6.78$ GHz and is coupled with an energy decay rate of $\kappa \approx 1/(37\ \text{ns})$ through a bandpass Purcell filter [20,24] to a 50 Ω output line and amplifiers.

Each transmon level $|i\rangle$ induces a different frequency shift on the resonator, yielding a set of distinct resonator frequencies $\omega_{r,|i\rangle}$. To measure the transmon state, we drive the system through the Purcell filter at a frequency between $\omega_{r,|1\rangle}$ and $\omega_{r,|2\rangle}$ [26], populating the resonator with photons that leak out from the resonator, through the filter, and into the amplifier circuit. The amplitude and phase of the outgoing photons are shifted (dispersed) in a way that depends on the resonator frequency, and thus the transmon state. We digitize this signal and extract the amplitude and phase as a point in the IQ plane. In Fig. 1(b), we plot the IQ response of the resonator with the transmon prepared in various states, which acts as our calibration for distinguishing the state of the transmon in subsequent measurements. When the resonator-transmon detuning $|\Delta| \equiv |\omega_{10} - \omega_r|$ is not more than 1.4 GHz, the resulting IQ points resolve up to the first four transmon states, while at larger $|\Delta|$ (relevant to most of our data) we can only resolve the first three states due to the smaller dispersive shift.

To investigate the effect of resonator photons on the transmon state, we use the pulse sequence illustrated in Fig. 2(a). The transmon is initialized to $|0\rangle$ by idling for several times its energy decay lifetime. We first drive the resonator with a 2 μs long, variable power pulse. This "stimulation pulse" injects a number of photons into the resonator that, when large enough, induces transitions in the transmon state. We then wait 500 ns (13 decay time constants) for the resonator to ring down [27]. Finally, we drive the resonator again with a fixed low power pulse to measure the transmon without inducing further transitions, and record the IQ response of the resonator. Based on the calibration shown in Fig. 1(d), we identify each IQ point as one of the transmon states, or if the point is more than three standard deviations from any of the calibrated distributions, we label it as an "outlier".

The results are striking in two ways. First, as the stimulation pulse power is raised, the transmon jumps from $|0\rangle$ not only to $|1\rangle$ but also to $|2\rangle$, $|3\rangle$ and even higher states, as shown in Fig. 2(b). Although we can resolve only up to $|3\rangle$, the characteristic arc of the IQ points with increasing state index appears to continue to what we estimate to be $|5\rangle$ or higher. Second, the probability of transitions is highly nonmonotonic with power, as was previously seen in Refs. [18,19]. In particular, the shapes of the features in probability versus power resemble resonance peaks, with large peaks in the outlier probability at drive powers 0.7 (feature A) and 0.2 (feature B), a small peak in

$|1\rangle$ near 0.15, another small peak in $|2\rangle$ near 0.05, and various other peaks at other powers. The peaked structure rules out any process that would have monotonically increasing transitions with increasing drive power, such as chip heating or dressed dephasing [31,32], as the dominant mechanism.

In order to connect our results to theoretical models, we next convert stimulation pulse power to photon number $\overline{n}$. We cannot measure $\overline{n}$ directly, but resonator photons cause the qubit frequency to shift downward in what is called the ac Stark effect [33]. We map drive power to $\overline{n}$ by measuring the ac Stark shifted qubit frequency for each resonator drive power and converting that frequency to $\overline{n}$ using a numerical model based on separately measured parameters g and Δ [28]. To measure the ac Stark shift, we repeat the previous experiment with the addition of a spectroscopic microwave pulse on the transmon after the driven resonator has reached the steady state. For each drive power we vary the frequency of the transmon pulse; the $|1\rangle$ probability is maximized when the pulse is on resonance with the shifted transmon frequency.

We show the results of the ac Stark shift measurement with the computed photon numbers in Fig. 2(d) for the same drive powers as in Fig. 2(c). Note that feature B (black dashed line) occurs at $170 \lesssim \overline{n} \lesssim 250$, which is, interestingly, considerably larger than the critical photon number $n_c \equiv (\Delta/g)^2/4 \approx 60$ introduced in Ref. [3].

The peaks in Fig. 2(c) are thus seen to indicate particular values of $\overline{n}$ at which the qubit-resonator system is especially susceptible to transitions. The association of $\overline{n}$ with qubit frequency shift further suggests that the peaks are due to some form of frequency resonance. With the observation of resonant transitions to higher transmon levels, we now consider the Hamiltonian of the transmon-resonator system and look for terms, possibly neglected in the dispersive or rotating wave approximations, which explain these observations.

We start with the bare Hamiltonian

$$H_b = \sum_k E_k |k\rangle\langle k| + \hbar\omega_r a^\dagger a, \qquad (1)$$

where E_k is the energy of transmon level k and ω_r is the frequency of the resonator. This Hamiltonian produces the JC ladder as shown by the solid lines in Fig. 3.

Adding the interaction term H_I due to the capacitive coupling gives

$$H_I = \sum_{k,k',n} \hbar g_{k,k'} \sqrt{n} |k', n-1\rangle\langle k, n| + \text{H.c.}, \qquad (2)$$

where the states are labeled $|\text{qubit}, \text{resonator}\rangle$, $g_{k,k'} = g\langle k|Q|k'\rangle/\langle 0|Q|1\rangle$, and $\langle k|Q|k'\rangle$ are the transmon charge matrix elements. This interaction imparts an n-dependent shift on the bare levels producing eigenstates, two of which are shown as dashed lines in Fig. 3. As indicated by the long horizontal arrow, at certain n the ladder contains

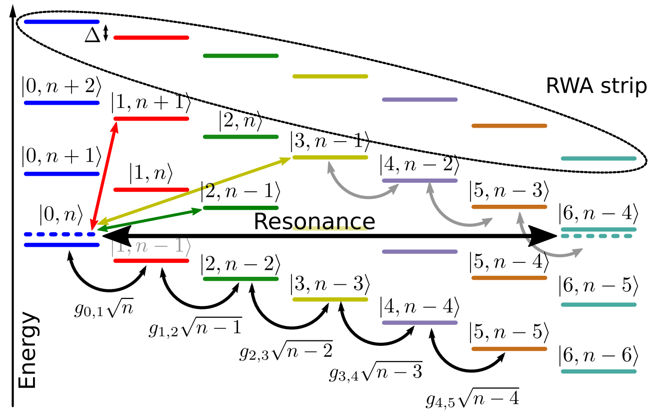

FIG. 3. JC ladder for large values of n. Bare states are shown as solid lines and two of the eigenstates are shown as dashed lines. Dark curved arrows indicate coupling within an RWA strip with corresponding RWA coupling strengths shown below. The ladder has an energy resonance between $|0, n\rangle$ and $|6, n-4\rangle$ (long black arrow). Non-RWA couplings (short straight arrows) allow for interstrip transitions. The couplings to $|1, n+1\rangle$ (red) and $|3, n-1\rangle$ (yellow), along with those within the RWA strip, mediate the transition between the resonant levels. The coupling to $|2, n-1\rangle$ (green), which mediates additional resonant transitions, requires a Hamiltonian term coupling transmon states of equal parity; this is forbidden if the transmon potential is symmetric. Note the energy spacing between states $|k, n\rangle$ and $|k+1, n-1\rangle$ is Δ as indicated in the top left.

resonances between states where the qubit goes from $|0\rangle$ to higher levels such as $|6\rangle$. This critical observation could explain both the resonance structure and the transitions to higher transmon levels observed in the data. However, it remains to see how H_I couples the resonant levels.

The full interaction H_I is typically simplified by the RWA to contain only those terms that preserve excitation number,

$$H_{\text{RWA}} \equiv \sum_{k,n} \hbar g_{k,k+1} \sqrt{n} |k+1, n-1\rangle\langle k, n| + \text{H.c.} \qquad (3)$$

These terms (curved arrows in Fig. 3) divide the JC ladder into excitation preserving subspaces that we call "RWA strips." Under H_{RWA}, the system moves only *within* an RWA strip; taking the system out of the dispersive limit with $n \gg n_c$ *only* results in a reduction of the resonator dispersive shift [21,28]. Therefore, H_{RWA} does not allow transitions between resonant levels.

The critical part of the Hamiltonian is $H_{\text{non-RWA}}$, containing terms in H_I that do not conserve excitation number [28]. These terms can be as large as the RWA terms, but are usually neglected on the grounds that they are more off resonant than the RWA terms (in our system the RWA terms are ~1 GHz off resonance, while the non-RWA terms are ~13 GHz off resonance). However, keeping these terms reveals the essential reason for the unwanted state transitions. The non-RWA terms couple next-nearest neighboring RWA strips (i.e., those differing by 2 in total excitation number) together, as shown in Fig. 3. Combined with the intrastrip coupling provided by H_{RWA}, the non-RWA coupling allows multistep (i.e., higher order) processes to connect the resonant levels. For example, $H_{\mathrm{non-RWA}}$ carries the system from $|0,n\rangle$ to $|1,n+1\rangle$ in another RWA strip, and then H_{RWA} carries the system within the strip to $|6,n-4\rangle$. Note that although the full process conserves energy, the individual steps do not.

To find the condition under which the resonances occur, we numerically compute the frequencies $\overline{\omega}_k(n) \equiv E_{\overline{|k,n-k\rangle}}/\hbar - n\omega_r$ (the overline indicates eigenstate) of the levels within each RWA strip, as functions of n. As n increases, energy levels within each strip repel each other more strongly and fan out, as illustrated by the solid lines in the "fan diagram" in Fig. 4(a). By superimposing fan diagrams of two next-nearest neighboring RWA strips, as shown by the dashed lines, we see that they have multiple intersections, meaning that the JC ladder contains multiple resonances. For example, the left red dot in Fig. 4 (a) shows that the transmon-resonator state $|0,n\rangle$ can be brought on resonance with $|6,n-4\rangle$. The presence of crossings with higher transmon states agrees with the experimental observation of transitions to states higher than $|3\rangle$.

Next, we compute the n at which various intersections occur as a function of the qubit-resonator detuning Δ, yielding the lines in Fig. 4(b). As $|\Delta|$ increases, the spacing between levels within an RWA strip also increases; see Fig. 3. However, the spacing between strips is fixed at ω_r, so with increased $|\Delta|$ fewer photons are required to bring $|0,n\rangle$ on resonance with states in higher strips and so the transitions occur at lower $\overline{n}$. Note that while we use n in the theory, the experiment drives the resonator into a coherent state with mean photon number $\overline{n}$ and fluctuations $\sqrt{\overline{n}} < 0.1\overline{n}$. Also, although the n at which the energy resonance occurs is not related to n_c, the effective couplings between resonant levels are large enough to yield the experimental features only when $n \gtrsim n_c$.

To confirm the theoretical prediction, we repeat the experiment shown in Fig. 2 for several values of ω_{10} by biasing the transmon's SQUID with magnetic flux. At each ω_{10}, we find the values of $\overline{n}$ of features A and B [as shown in Fig. 2(d)] and plot these points in Fig. 4(b). The experimental points for feature A (black circles) and feature B (blue squares) are well fit by numerically computed curves for the transitions from $|0,n\rangle$ to $|6,n-4\rangle$ and $|3,n-2\rangle$, respectively. Note that the theory lines are calculated using only the measured ω_r, ω_{10}, and g, with no free parameters fitted to the data.

However, the transition from $|0,n\rangle$ to $|3,n-2\rangle$ is actually unexpected. If the transmon potential is symmetric, as is usually assumed [5], then $g_{i,j}$ is only nonzero when $j-i$ is odd. Therefore, H_I should only couple RWA strips where the difference in total excitation number is even, so the transition to $|3,n-2\rangle$ should be forbidden. Nevertheless, the theory

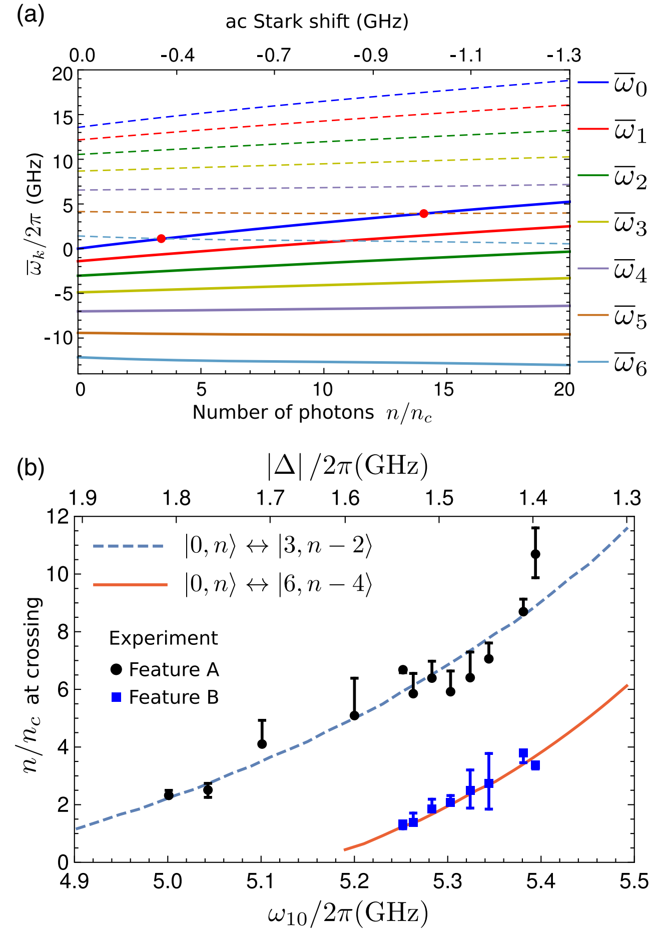

FIG. 4. (a) Fan diagram of the energy levels within an RWA strip. Solid: Frequencies $\bar{\omega}_k(n) \equiv E_{\overline{|k,n-k\rangle}}/\hbar - n\omega_r$ versus photon number n for $|\Delta| = 1.4$ GHz. As n increases, the levels repel more strongly and fan out. Dashed: Same frequencies shifted by $2\omega_r$, which represent the next-nearest neighboring RWA strip. The red dots show energy resonances with the qubit state $|0\rangle$ occurring at specific values of n. The left dot corresponds to the resonance shown in Fig. 3. (b) Photon number at level crossing versus ω_{10}, compared between experiment and theory. Black circles and blue squares show experimental features A and B from Fig. 2, respectively, and the error bars represent the apparent widths of the features. The solid red line is the theory prediction for level crossing between eigenlevels of $|0,n\rangle$ and $|6,n-4\rangle$. The dashed blue line is the theory prediction for an asymmetric transmon that breaks the selection rule by at least 1%, yielding level crossings between eigenlevels of $|0,n\rangle$ and $|3,n-2\rangle$.

line for the $|3,n-2\rangle$ transition fits the data well, indicating a possible asymmetry in the transmon potential. We confirmed this asymmetry by observing $|0\rangle \to |2\rangle$ Rabi oscillations when driving the transmon at $\omega_{01} + \omega_{12}$ [28]. Through comparison with Rabi oscillations on the $|0\rangle \to |1\rangle$ transition, we experimentally estimate $|\langle 0|Q|2\rangle / \langle 0|Q|1\rangle| \approx 10^{-2}$ [28]. This matrix element is large enough to explain the transitions to $|3,n-2\rangle$, and so the level crossing theory appears to correctly predict both of the largest resonance features observed in the data.

We note that any spurious TLS coupled to the transmon-resonator system can also participate in level crossings, and can lead to similar features [possibly the small peaks in Fig. 2(c)], even at lower photon numbers [28].

In conclusion, we find that strong dispersive measurement of a transmon induces transitions to states above $|3\rangle$. These transitions occur at specific values of the photon occupation in the measurement resonator, and are caused by energy resonances within the qubit-resonator system. Coupling between the resonant levels is mediated by Hamiltonian terms usually dropped in the rotating wave approximation, and the most important such term involves an unexpected broken symmetry in the transmon potential. An interesting consequence of these results is that a system with smaller $|\Delta|$ should allow larger photon numbers before resonant transitions occur. This observation could be critical to improving measurement accuracy in dispersively measured systems, and may explain the large photon numbers used in Ref. [34]. This work suggests several further avenues of research: characterizing level crossings with the qubit initialized in $|1\rangle$, determining the mechanism for the transmon's broken symmetry, clarifying the role of TLSs in non-RWA transitions, and understanding the n-dependent rates of the non-RWA transitions.

The authors thank C. Bultink for an enlightening discussion. This work was supported by Google. Z. C. and C. Q. acknowledge support from the National Science Foundation (NSF) Graduate Research Fellowship under Grant No. DGE 1144085. M. K. and A. N. K. acknowledge support from ARO Grants No. W911NF-15-1-0496 and No. W911NF-11-1-0268. Devices were made at the UC Santa Barbara Nanofabrication Facility, a part of the NSF-funded National Nanotechnology Infrastructure Network, and at the Nanostructures Cleanroom Facility.

D. S., Z. C., and M. K. contributed equally to this work.

*sank.daniel@gmail.com

[1] E. T. Jaynes and F. W. Cummings, IEEE Proc. **51**, 89 (1963).
[2] M. Tavis and F. W. Cummings, Phys. Rev. **170**, 379 (1968).
[3] A. Blais, R.-S. Huang, A. Wallraff, S. M. Girvin, and R. J. Schoelkopf, Phys. Rev. A **69**, 062320 (2004).
[4] A. Wallraff, D. I. Schuster, A. Blais, L. Frunzio, R.-S. Huang, J. Majer, S. Kumar, S. M. Girvin, and R. J. Schoelkopf, Nature (London) **431**, 162 (2004).
[5] J. Koch, T. M. Yu, J. Gambetta, A. A. Houck, D. I. Schuster, J. Majer, A. Blais, M. H. Devoret, S. M. Girvin, and R. J. Schoelkopf, Phys. Rev. A **76**, 042319 (2007).
[6] K. Murch, S. Weber, C. Macklin, and I. Siddiqi, Nature (London) **502**, 211 (2013).
[7] S. J. Weber, A. Chantasri, J. Dressel, A. N. Jordan, K. W. Murch, and I. Siddiqi, Nature (London) **511**, 570 (2014).
[8] M. Hatridge, S. Shankar, M. Mirrahimi, F. Schackert, K. Geerlings, T. Brecht, K. M. Sliwa, B. Abdo, L. Frunzio, S. M. Girvin, R. J. Schoelkopf, and M. H. Devoret, Science **339**, 178 (2013).
[9] R. Barends, J. Kelly, A. Megrant, A. Veitia, D. Sank, E. Jeffrey, T. White, J. Mutus, A. Fowler, B. Campbell *et al.*, Nature (London) **508**, 500 (2014).
[10] J. M. Chow, J. M. Gambetta, E. Magesan, D. W. Abraham, A. W. Cross, B. R. Johnson, N. A. Masluk, C. A. Ryan, J. A. Smolin, S. J. Srinivasan, and M. Steffen, Nat. Commun. **5**, 4015 (2014).
[11] F. Yan, J. Bylander, S. Gustavsson, F. Yoshihara, K. Harrabi, D. G. Cory, T. P. Orlando, Y. Nakamura, J.-S. Tsai, and W. D. Oliver, Phys. Rev. B **85**, 174521 (2012).
[12] J. Kelly, R. Barends, A. G. Fowler, A. Megrant, E. Jeffrey, T. C. White, D. Sank, J. Y. Mutus, B. Campbell, Y. Chen, Z. Chen, B. Chiaro, A. Dunsworth, I. Hoi, C. Neill, P. J. J. O'Malley, C. Quintana, P. Roushan, A. Vainsencher, J. Wenner, A. N. Cleland, and J. M. Martinis, Nature (London) **519**, 66 (2015).
[13] A. D. Córcoles, E. Magesan, S. J. Srinivasan, A. W. Cross, M. Steffen, J. M. Gambetta, and J. M. Chow, Nat. Commun. **6**, 6979 (2015).
[14] D. Ristè, S. Poletto, M.-Z. Huang, A. Bruno, V. Vesterinen, O.-P. Saira, and L. DiCarlo, Nat. Commun. **6**, 6983 (2015).
[15] D. Ristè, C. C. Bultink, M. J. Tiggelman, R. N. Schouten, K. W. Lehnert, and L. DiCarlo, Nat. Commun. **4**, 1913 (2013).
[16] A. G. Fowler, M. Mariantoni, J. M. Martinis, and A. N. Cleland, Phys. Rev. A **86**, 032324 (2012).
[17] M. D. Reed, L. DiCarlo, B. R. Johnson, L. Sun, D. I. Schuster, L. Frunzio, and R. J. Schoelkopf, Phys. Rev. Lett. **105**, 173601 (2010).
[18] J. E. Johnson, C. Macklin, D. H. Slichter, R. Vijay, E. B. Weingarten, J. Clarke, and I. Siddiqi, Phys. Rev. Lett. **109**, 050506 (2012).
[19] D. Sank, Ph. D. thesis, Univeristy of California Santa Barbara, 2014.
[20] E. Jeffrey, D. Sank, J. Y. Mutus, T. C. White, J. Kelly, R. Barends, Y. Chen, Z. Chen, B. Chiaro, A. Dunsworth, A. Megrant, P. J. J. O'Malley, C. Neill, P. Roushan, A. Vainsencher, J. Wenner, A. N. Cleland, and J. M. Martinis, Phys. Rev. Lett. **112**, 190504 (2014).
[21] M. Khezri, E. Mlinar, J. Dressel, and A. N. Korotkov, Phys. Rev. A **94**, 012347 (2016).
[22] R. Barends, J. Kelly, A. Megrant, D. Sank, E. Jeffrey, Y. Chen, Y. Yin, B. Chiaro, J. Mutus, C. Neill, P. O'Malley, P. Roushan, J. Wenner, T. C. White, A. N. Cleland, and J. M. Martinis, Phys. Rev. Lett. **111**, 080502 (2013).
[23] Coupling strength depends on ω_{10}, but varies by less than 5% in this work.
[24] M. Reed, B. Johnson, A. Houck, L. DiCarlo, J. Chow, D. Schuster, L. Frunzio, and R. Schoelkopf, Appl. Phys. Lett. **96**, 203110 (2010).
[25] J. Y. Mutus, T. C. White, R. Barends, Y. Chen, Z. Chen, B. Chiaro, A. Dunsworth, J. Jeffrey, E. Kelly, A. Megrant, C. Neill, P. J. J. O'Malley, P. Roushan, D. Sank, A. Vainsencher, J. Wenner, K. M. Sundqvist, A. N. Cleland, and J. M. Martinis, Appl. Phys. Lett. **104**, 263513 (2014).

[26] This choice of frequency maximizes the visibility of the lowest three transmon states.
[27] The transmon T_1 is between 20 and 40 μs for the ω_{10} values used, so the resonator ring down incurs little qubit decay.
[28] See Supplemental Material at http://link.aps.org/supplemental/10.1103/PhysRevLett.117.190503 for detailed analysis of the system Hamiltonian, $|0\rangle \rightarrow |2\rangle$ coupling, and TLS assisted transitions, which includes Refs. [29,30].
[29] É. Dumur, B. Küng, A. Feofanov, T. Weißl, Y. Krupko, N. Roch, C. Naud, W. Guichard, and O. Buisson, IEEE Trans. Appl. Supercond. **26**, 1700304 (2016).
[30] J. M. Martinis, K. B. Cooper, R. McDermott, M. Steffen, M. Ansmann, K. D. Osborn, K. Cicak, S. Oh, D. P. Pappas, R. W. Simmonds, and C. C. Yu, Phys. Rev. Lett. **95**, 210503 (2005).
[31] M. Boissonneault, J. M. Gambetta, and A. Blais, Phys. Rev. A **77**, 060305 (2008).
[32] D. H. Slichter, R. Vijay, S. J. Weber, S. Boutin, M. Boissonneault, J. M. Gambetta, A. Blais, and I. Siddiqi, Phys. Rev. Lett. **109**, 153601 (2012).
[33] D. I. Schuster, A. Wallraff, A. Blais, L. Frunzio, R.-S. Huang, J. Majer, S. M. Girvin, and R. J. Schoelkopf, Phys. Rev. Lett. **94**, 123602 (2005).
[34] C. C. Bultink, M. A. Rol, T. E. O'Brien, X. Fu, B. C. S. Dikken, R. Vermeulen, J. C. de Sterke, A. Bruno, R. N. Schouten, and L. DiCarlo, Phys. Rev. Applied **6**, 034008 (2016).